JOURNAL OF SPACECRAFT AND ROCKETS
Vol. 39, No. 2, March–April 2002

# Local Effects of Piezopolymer Patches on Inflatable Space-Based Structures

R. Brett Williams*
*Virginia Polytechnic Institute and State University, Blacksburg, Virginia 24061*
Eric M. Austin†
*Clemson University, Clemson, South Carolina 29634*
and
Daniel J. Inman‡
*Virginia Polytechnic Institute and State University, Blacksburg, Virginia 24061*

**Inflatable structures are often characterized as membranes (that is, structural elements that cannot resist bending moments). This simplification raises the question of whether membrane theory can account for the effects of active, surface-mounted piezopolymer patches. This work discusses these effects on the dynamic behavior of a flat, rectangular coupon section and assesses the patch's ability to sense and actuate transverse deflections of the thin-film substrate using traditional membrane theory. The Rayleigh–Ritz method was employed to approximate the natural frequencies and mode shapes of this layered system. Although including the additional mass of the patch, traditional membrane theory was unable to account for the added stiffness of the patch layer. When the piezoelectric behavior of the patch was considered, membrane theory failed to model the piezopolymer as a useful sensor. Also, excitation of transverse vibrations was not possible using membrane theory, which does not allow application of bending moments. However, piezoelectric actuation was modeled as applied in-plane forces, which enabled the patch to suppress out-of-plane disturbances by altering the tension in the base layer as a function of applied voltage.**

## Nomenclature

| | | |
|---|---|---|
| $a$ | = | $x$ dimension of Kapton base layer |
| $\boldsymbol{a}$ | = | Rayleigh–Ritz constants |
| $a_P$ | = | $x$ dimension of polylvinylidene fluoride (PVDF) patch layer |
| $b$ | = | $y$ dimension of Kapton base layer |
| $b_P$ | = | $y$ dimension of PVDF patch layer |
| $\mathrm{d}A$ | = | unstretched area of membrane |
| $\mathrm{d}A'$ | = | stretched area of membrane |
| $\mathrm{d}s$ | = | stretched length of differential membrane element |
| $\mathrm{d}x$, $\mathrm{d}y$ | = | unstretched dimensions of differential membrane element |
| $E_b$, $E_P$ | = | elastic modulus |
| $H$ | = | Heaviside's function |
| $I$ | = | functional from Hamilton's principle |
| $K$ | = | kinetic energy |
| $k_{ij}$ | = | stiffness matrix |
| $L$, $M$ | = | differential operators |
| $M$, $N$ | = | maximum number of waves |
| $m$, $n$ | = | wave number |
| $m_{ij}$ | = | mass matrix |
| $P$ | = | $x$- and $y$-direction tensions (force per unit length) |
| $p$ | = | internal pressure of torus |
| $R$ | = | variable radial location on torus |
| $r_1$ | = | minor radius of the torus |
| $T$ | = | thickness (with subscript) |
| $t$ | = | time (no subscript) |
| $U$ | = | strain energy |
| $u_i$ | = | comparison functions |
| $w$ | = | transverse deflection |
| $x$, $y$ | = | rectangular Cartesian coordinates |
| $x_1$, $y_1$ | = | coordinates of bottom-left-hand corner of patch |
| $x_2$, $y_2$ | = | coordinates of top-right-hand corner of patch |
| $\varepsilon_x$, $\varepsilon_y$ | = | strain |
| $\kappa$ | = | geometric constant relating $\sigma_x$ and $\sigma_y$ |
| $\rho_b$, $\rho_P$ | = | density per unit area |
| $\rho_m$, $\rho_{mP}$ | = | mass density per unit volume |
| $\sigma_x$, $\sigma_y$ | = | normal stress or component of stress tensor |
| $\omega_{ij}$ | = | natural frequency |

*Active Material Notation*

| | | |
|---|---|---|
| $C_p$ | = | capacitance of PVDF |
| $D_i$ | = | electric displacement tensor |
| $d_{ijk}$ | = | piezoelectric constant tensor |
| $E_j$ | = | applied electric field tensor |
| $P$ | = | poling direction (Fig. 5) |
| $S_{ij}$ | = | strain tensor |
| $s^E_{ijkl}$ | = | elastic compliance tensor |
| $T_{jk}$ | = | stress tensor |
| $V$ | = | voltage |
| $Y_P$ | = | elastic modulus |
| $\varepsilon^T_{ij}$ | = | permittivity tensor, at constant stress |

Received 22 March 2001; revision received 12 November 2001; accepted for publication 18 November 2001. 

*Graduate Research Assistant, Center for Intelligent Material Systems and Structures, Department of Mechanical Engineering, 310 Durham Hall; rowilli6@vt.edu.

†Assistant Professor, Department of Mechanical Engineering, 218 Fluor Daniel Building, Box 340921; ema@clemson.edu. Senior Member AIAA.

‡G. R. Goodson Professor and Director, Center for Intelligent Material Systems and Structures, Department of Mechanical Engineering; dinman@vt.edu. Associate Fellow AIAA.

## Introduction

INFLATABLE space-based devices have become popular over the past three decades because of their minimal launch mass and launch volume. Once inflated, these space structures are subject to vibrations induced mechanically by guidance systems and space debris as well as thermally induced vibrations from variable amounts of direct sunlight during orbit around the Earth. Controlling the vibrations of spaced-based structures is critical to ensuring optimal performance. Some work has been performed concerning the dynamic behavior of inflated structures, from simple systems such as thin-walled cantilevered tubes[1] to full toroidal shells[2] to

entire inflated satellites.[3] Each of these works focused on modeling and experimental modal analysis of such inflated structures. As far as intelligent structures are concerned, there exists a vast body of literature dealing with the interaction between piezoelectric devices and their host structure.

There exist simple models such as the pin force[4] and enhanced pin-force methods[5] as well as more detailed representations that consider finite thickness bonding layers[6] and excitation and control of the bending responses of beams,[7] plates,[8] and shells.[8] Building from these models of piezostructure interactions, control schemes have been developed for thin, layered membrane structures to actively reduce the transient noise transmission in a circular duct.[9] Also, polyvinylidene fluoride (PVDF) patches have been used to excite inflated torus structures for modal testing.[10] Although this actuation has proved possible in a laboratory environment, using traditional membrane theory to model such thin structures with piezoelectric attachments has been shown to be severely limited.[11] A finite element analysis of an entire inflated toroidal shell using plate elements has shown that the PVDF patches have essentially no effect on the natural frequencies and mode shapes of the system.[12]

The current research effort supports a program to model and develop an active control system using smart materials to suppress the vibrations of inflatable communication satellites. These structures typically consist of three inflated struts that connect an inflated torus structure supporting a membrane reflector to a communication and navigation hardware assembly. The passive influence of small piezoceramic devices attached to metal host structures is typically ignored. However, a piezopolymer (PVDF) film attached to a thin, polyimide film such as Kapton® for the satellite at hand could greatly change the mass and stiffness values in the area under and around the patch, thus altering the dynamic behavior of the satellite. This article assesses these changes as well as identifies the many limitations associated with using traditional membrane theory to analyze the dynamic behavior of thin, layered systems.

## Stress Analyses

### Inflatable Torus

The first step in investigating inflatable structures is to use thin-wall pressure vessel theory to assess the stresses that develop in the material as a result of the internal pressure. A rectangular portion of the structure is then isolated and presumed to be flat for the analysis at hand as shown in Fig. 1.

Clearly, this coupon is in a state of plane stress with zero in-plane shear. Furthermore, the calculated stresses at a given point are presumed to be constant along the edge of the coupon despite a small variation in radial location on the torus. This approximation is reasonable because, for typical inflatable satellite geometries, the actual values of stress only vary a few percent from the inner to outer radius of the torus. If a rectangular PVDF patch is perfectly bonded to the center of this coupon, the layered system would appear as shown in Fig. 2.

The edge stresses far away from the patch seen in Fig. 2 are given by the following relationships:

$$\sigma_x = pr_1/2t_b \tag{1}$$

$$\sigma_y = (pr_1/2t_b)[(R + r_t)/R] = \sigma_x \kappa \tag{2}$$

### Layered Coupon

The resultant forces in the PVDF patch and the rigidly bonded substrate directly beneath it must be in equilibrium with those forces

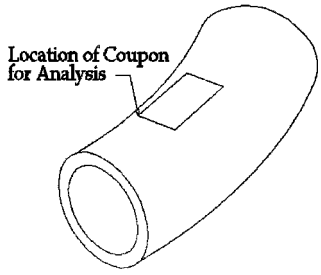


**Fig. 1 Selected coupon.**

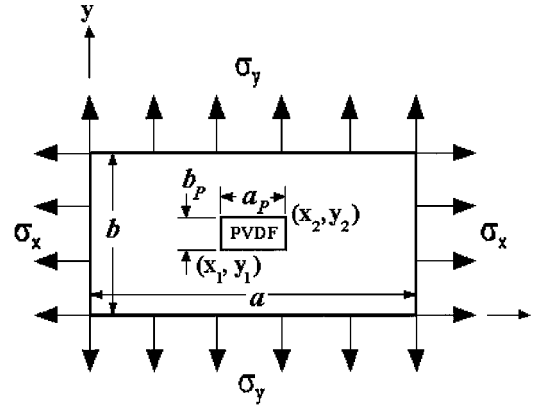


**Fig. 2 Layered coupon with direction-dependent stresses.**

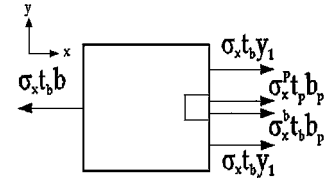


***x*-direction forces**

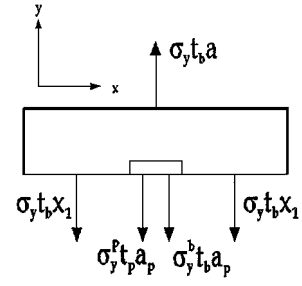


***y*-direction forces**

**Fig. 3 Free-body diagrams of layered system.**

in the surrounding coupon. That is, the stresses in the pressure vessel walls are different within and outside of the region of the PVDF patch. This variation in stress can be modeled simply with step functions, which suggests that there exist three distinct regions where the $x$ and $y$ values of stress must be calculated. These stresses are defined in the patch layer as $\sigma_x^P$ and $\sigma_y^P$, in the base layer under the patch as $\sigma_x^b$ and $\sigma_y^b$, and in the base layer away from the patch as $\sigma_x$ and $\sigma_y$.

Analysis of the inflated torus as a pressure vessel yielded values for $\sigma_x$ and $\sigma_y$, but four stresses remain unknown. However, using step approximations allows the various stresses to be treated as constants. This approach simplifies the strain energy analysis, as will become apparent in the next section, and allows free-body diagrams to be constructed of the layered system, as shown in Fig. 3.

Summations of these forces in the $x$ and $y$ directions yields two equilibrium equations:

$$\sigma_x t_b b = 2\sigma_x t_b y_1 + \sigma_x^b t_b b_P + \sigma_x^P t_P b_P \tag{3}$$

$$\sigma_y t_b a = 2\sigma_y t_b x_1 + \sigma_y^b t_b a_P + \sigma_y^P t_P a_P \tag{4}$$

This system is statically indeterminate (that is, has more unknowns than equilibrium equations), and so a deformation analysis must be performed to provide more governing equations. Because this system is in a biaxial state of stress, the corresponding form of Hooke's law can be used to calculate the strains in the patch layer and base layer under the patch. Assuming the patch is rigidly bonded to the base layer under the patch, the layers must deform by equal amounts. Because these regions have the same size, by definition the $x$ and $y$ strains are equated such that

$$\varepsilon_x : (1/E_b)\left(\sigma_x^b - \nu_b \sigma_y^b\right) = (1/E_P)\left(\sigma_x^P - \nu_P \sigma_y^P\right) \tag{5}$$

$$\varepsilon_y : (1/E_b)\left(\sigma_y^b - \nu_b \sigma_x^b\right) = (1/E_P)\left(\sigma_y^P - \nu_P \sigma_x^P\right) \tag{6}$$

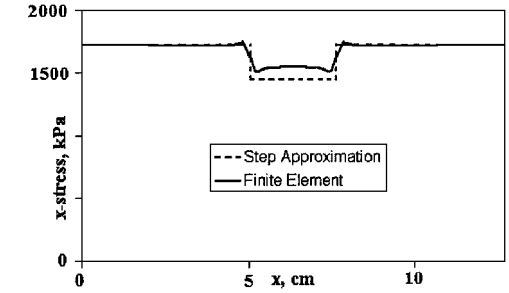


*x*-direction base-layer stresses

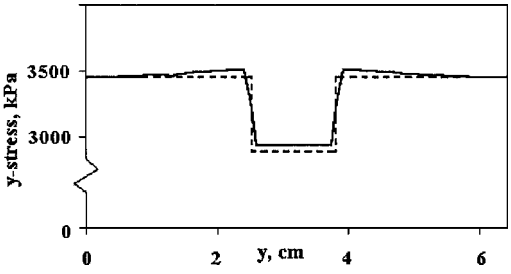


*y*-direction base-layer stresses

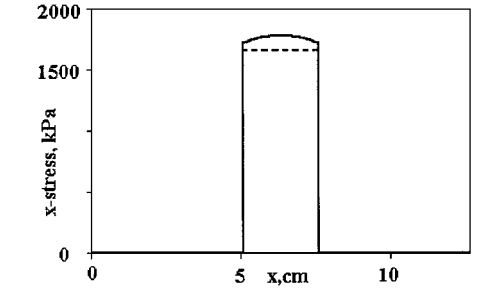


*x*-direction patch-layer stresses

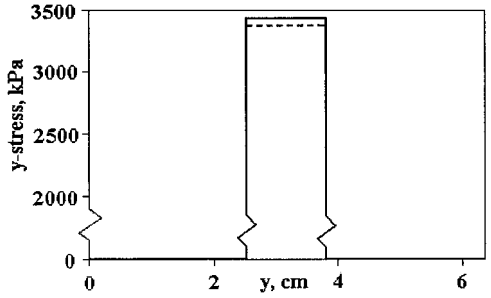


*y*-direction patch-layer stresses

**Fig. 4 Verification of step approximation for membrane stresses.**

This set of four equations and four unknowns, derived from the step changes in stress approximation, can now be solved simultaneously for the desired stresses. The resulting equations are quite lengthy and, in interest of brevity, have been omitted. Instead, a numerical calculation was made, and the results appear in Fig. 4 along with a comparison with values generated from an ANSYS static finite element model of a $12.7 \times 6.35 \times 0.00762$ cm Kapton substrate with a $2.54 \times 1.27 \times 0.00127$ cm PVDF patch rigidly bonded and centered as depicted in Fig. 2. SHELL41 membrane elements were used to construct the model, and the edge loads, $\sigma_x$ and $\sigma_y$ from Eqs. (1) and (2), were 3.45 and 1.72 MPa, respectively.

From Fig. 4 it is clear that using step approximations to represent the stresses at various regions of the layered system produces a simplified analysis and reasonable results.

## Dynamic Analysis with Passive PVDF Patch

With the state of stress known at all points in both layers, the equation of motion for the layered system can now be derived using Hamilton's principle. A Rayleigh–Ritz solution is then used to approximate the natural frequencies and mode shapes.

**Kinetic Energy**

For the geometry defined in Fig. 2, the kinetic energy is found to be

$$K = \int_0^b \int_0^a \frac{\rho_b}{2}\left(\frac{\partial w}{\partial t}\right)^2 \mathrm{d}x\,\mathrm{d}y + \int_{y_1}^{y_2}\int_{x_1}^{x_2} \frac{\rho_P}{2}\left(\frac{\partial w}{\partial t}\right)^2 \mathrm{d}x\,\mathrm{d}y \quad (7)$$

However, because the patch does not necessarily cover the entire base layer, Heaviside functions are used to size and locate the patch, thereby simplifying the kinetic energy to a single area integral:

$$K = \frac{1}{2}\int_0^b \int_0^a \left(\frac{\partial w}{\partial t}\right)^2 \{\rho_b + \rho_P[H(x-x_1) - H(x-x_2)][H(y-y_1) - H(y-y_2)]\}\,\mathrm{d}x\,\mathrm{d}y \quad (8)$$

**Strain Energy**

The strain energy for a membrane is defined as

$$U = \iint P(\mathrm{d}A' - \mathrm{d}A) \quad (9)$$

where $(\mathrm{d}A' - \mathrm{d}A)$ is the change in surface area (that is, stretching of the membrane) as a result of the initial tension (force per unit length). This tension, which is found by multiplying the stress by the material thickness, is normally assumed large compared to any additional tension caused by stretching, and so it is assumed constant and is thus not a function of strain in the membrane. However, the tension in the base membrane will be different in the area under the patch, and so the integral of the strain energy density must be broken into pieces corresponding to the separate geometric regions. Also, because the tensions are direction-dependent the total strain energy is the sum of the strain energies caused by stretching in the $x$ and $y$ directions, given, respectively, as

$$\begin{aligned} U_x = {} & \int_0^b \int_0^{x_1} \sigma_x t_b(\mathrm{d}s_x - \mathrm{d}x)\,\mathrm{d}y + \int_0^{y_1}\int_{x_1}^{x_2} \sigma_x t_b(\mathrm{d}s_x - \mathrm{d}x)\,\mathrm{d}y \\ & + \int_{y_1}^{y_2}\int_{x_1}^{x_2} \left(\sigma_x^b t_b + \sigma_x^P t_P\right)(\mathrm{d}s_x - \mathrm{d}x)\,\mathrm{d}y \\ & + \int_{y_2}^{b}\int_{x_1}^{x_2} \sigma_x t_b(\mathrm{d}s_x - \mathrm{d}x)\,\mathrm{d}y + \int_0^b \int_{x_2}^{a} \sigma_x t_b(\mathrm{d}s_x - \mathrm{d}x)\,\mathrm{d}y \end{aligned} \quad (10)$$

$$\begin{aligned} U_y = {} & \int_0^b \int_0^{x_1} \sigma_y t_b(\mathrm{d}s_y - \mathrm{d}y)\,\mathrm{d}x + \int_0^{y_1}\int_{x_1}^{x_2} \sigma_y t_b(\mathrm{d}s_y - \mathrm{d}y)\,\mathrm{d}x \\ & + \int_{y_1}^{y_2}\int_{x_1}^{x_2} \left(\sigma_y^b t_b + \sigma_y^P t_P\right)(\mathrm{d}s_y - \mathrm{d}y)\,\mathrm{d}x \\ & + \int_{y_2}^{b}\int_{x_1}^{x_2} \sigma_y t_b(\mathrm{d}s_y - \mathrm{d}y)\,\mathrm{d}x + \int_0^b \int_{x_2}^{a} \sigma_y t_b(\mathrm{d}s_y - \mathrm{d}y)\,\mathrm{d}x \end{aligned} \quad (11)$$

From the geometry of the layered system shown in Fig. 2, the dimensions of the base layer can be written as

$$b = 2y_1 + b_p \quad (12)$$

$$a = 2x_1 + a_p \quad (13)$$

which simplify the equilibrium conditions of Eqs. (3) and (4) to

$$\sigma_x t_b = \sigma_x^b t_b + \sigma_x^P t_P \quad (14)$$

$$\sigma_y t_b = \sigma_y^b t_b + \sigma_y^P t_P \quad (15)$$

Application of these two expressions to the third area integral (PVDF patch area) in Eqs. (10) and (11), respectively, reduces the strain energies to

$$U_x = \int_0^b \int_0^a \sigma_x t_b (\mathrm{d}s_x - \mathrm{d}x)\,\mathrm{d}y \tag{16}$$

$$U_y = \int_0^b \int_0^a \sigma_y t_b (\mathrm{d}s_y - \mathrm{d}y)\,\mathrm{d}x \tag{17}$$

which are identical to the expressions for a bare membrane with direction-dependent tensions.[10] Because the strain energy of the layered system is unaffected by the addition of a PVDF patch, the stiffness of the system predicted by traditional membrane theory is unaffected as well. Nevertheless, adding the energies in the $x$ and $y$ directions, and using a binomial expansion to approximate the stretched length of a differential element in the $x$ and $y$ directions, yields the total strain energy expression

$$U = \frac{1}{2}\iint P_x \left[ \left( \frac{\partial w}{\partial x} \right)^2 + \kappa \left( \frac{\partial w}{\partial y} \right)^2 \right] \mathrm{d}x\,\mathrm{d}y \tag{18}$$

**Hamilton's Principle**

Using the energy expressions of Eqs. (8) and (18) for the layered system at hand, the partial differential equation of motion and boundary conditions for the layered system are found by applying Hamilton's principle, which states that the actual path of motion for a conservative system between two points in time $t_1$ and $t_2$ will extremize the functional:

$$I = \int_{t_1}^{t_2} (K - U)\,\mathrm{d}t \tag{19}$$

Setting the first variation of Eq. (19) equal to zero, the equation of motion for free vibrations in the transverse direction for the layered system, minus the stiffness effects of the patch, is

$$\{\rho_b + \rho_P [H(x - x_1) - H(x - x_2)][H(y - y_1) - H(y - y_2)]\} \times \left( \frac{\partial^2 w}{\partial t^2} \right) - P_x \left[ \left( \frac{\partial^2 w}{\partial x^2} \right) + \kappa \left( \frac{\partial^2 w}{\partial y^2} \right) \right] = 0 \tag{20}$$

and fixed boundary conditions are selected along all four edges of the base layer. This expression is a complicated partial differential equation of motion, and in the interest of simplicity various less complicated approximation techniques, namely the Rayleigh–Ritz and finite element methods, are used to extract modal information in lieu of a closed-form solution.

**Rayleigh–Ritz Method**

The Rayleigh–Ritz method uses assumed mode shapes of a complicated structure to approximate natural frequencies and mode shapes without directly solving the equation of motion. The mode shapes of a bare membrane are used as basis functions for the layered system:

$$w_i = \sum_{i=1}^{M*N} \boldsymbol{a}_i u_i = \sum_{m=1}^{M} \sum_{n=1}^{N} \boldsymbol{a}_{mn} \sin\left( \frac{m\pi x}{a} \right) \sin\left( \frac{n\pi y}{b} \right) \qquad i = 1, 2, \ldots, M \times N \tag{21}$$

Assumed mode shapes of this form are indicative of harmonic motion, for which equating the maximum values of kinetic and strain energy leads to the following expression for natural frequencies:

$$\omega_{ij}^2 = \frac{\int_0^b \int_0^a w_i L[w_j]\,\mathrm{d}x\,\mathrm{d}y}{\int_0^b \int_0^a w_i M[w_j]\,\mathrm{d}x\,\mathrm{d}y} \tag{22}$$

Although this form is mathematically accurate, subsequent numerical calculations using *Mathematica* are more efficient if the denominator is reverted back to the form of Eq. (7), giving

$$\omega_{ij}^2 = \frac{\int_0^b \int_0^a w_i L[w_j]\,\mathrm{d}x\,\mathrm{d}y}{\int_0^b \int_0^a w_i M^b[w_j]\,\mathrm{d}x\,\mathrm{d}y + \int_{y_1}^{y_2} \int_{x_1}^{x_2} w_i M^P[w_j]\,\mathrm{d}x\,\mathrm{d}y} \tag{23}$$

where $L$, $M^P$, and $M^b$ are given by

$$L = -P_x \left[ \left( \frac{\partial^2}{\partial x^2} \right) + \kappa \left( \frac{\partial^2}{\partial y^2} \right) \right], \qquad M^b = \rho_b, \qquad M^P = \rho_P \tag{24}$$

With these operators defined, the mass and stiffness matrices are given by

$$k_{ij} = \int_0^b \int_0^a u_i L[u_j]\,\mathrm{d}x\,\mathrm{d}y$$

$$m_{ij} = \int_0^b \int_0^a u_i M^b[u_j]\,\mathrm{d}x\,\mathrm{d}y + \int_{y_1}^{y_2} \int_{x_1}^{x_2} u_i M^P[u_j]\,\mathrm{d}x\,\mathrm{d}y \tag{25}$$

At this point the mass and stiffness matrices can be calculated, thereby reducing the distributed parameter layered membrane system to one with a finite number of degrees of freedom. A numerical example will be considered later and compared with a finite element analysis.

**Finite Element Method**

Figure 5 depicts the ANSYS finite element model that was constructed to approximate the natural frequencies and mode shapes of the layered system and to verify the Rayleigh–Ritz method already outlined.

The geometric and material properties for this model are listed in Tables 1 and 2 for the two different layers.

With the ANSYS geometry assembled, tensile pressure loads were applied to the edges according to Table 1, and a static solution was found along with a prestressed stiffness matrix. The resulting static stresses were used to construct Fig. 4, whereas the prestressed stiffness matrix was used in the subsequent modal analysis to account for the initial tension in the base layer. Next, the edge nodes were restricted from translation in any direction to simulate the fixed boundary conditions, and a modal analysis was performed in

**Table 1 Kapton base-layer properties**

| Property symbol | Value |
|---|---|
| $x$ dimension $a$ | 0.127 (5.0), m (in.) |
| $y$ dimension $b$ | 0.0635 (2.5), m (in.) |
| Thickness $t_b$ | 7.62$E$−05 (0.003), m (in.) |
| $P_x$ | 131.3 (0.75), N/m (1b/in.) |
| $\kappa$ | 2.0 |
| Mass density $\rho_{mb}$ | 1.42 (1.328$E$−04), g/cm$^3$ [(1b-s$^2$)/in.$^4$] |
| Elastic modulus $E_b$ | 2.55 (370), GPa (ksi) |
| Poisson's ratio $\nu_b$ | 0.34 |

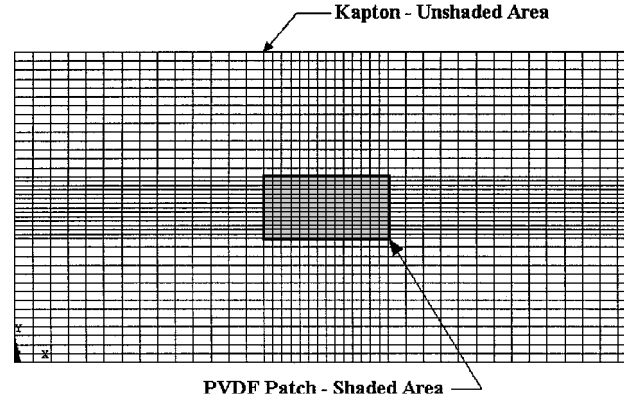


**Fig. 5 ANSYS finite element model of layered coupon.**

**Table 2 PVDF layer properties**

| Property symbol | Value |
|---|---|
| $x$ dimension $a_P$ | 0.0254 (1.0), m (in.) |
| $y$ dimension $b_P$ | 0.0127 (0.5), m (in.) |
| Thickness $t_P$ | 1.27$e$−05 (0.0005), m (in.) |
| $x_1$ | 0.0508 (2.0), m (in.) |
| $y_1$ | 0.0254 (1.0), m (in.) |
| Mass density $\rho_{mP}$ | 1.78 (1.651$E$−04), g/cm$^3$ [(1b-s$^2$)/in.$^4$] |
| Elastic modulus $E_P$ | 3.0 (435), GPa (ksi) |
| Poisson's ratio $\nu_P$ | 0.3 |

**Table 3 First 10 natural frequencies of layered system**

| | | Natural frequency, Hz | | Percent |
|---|---|---|---|---|
| $m$ | $n$ | Rayleigh–Ritz method[a] | Finite element method[b] | difference (RR-FEA) |
| 1 | 1 | 405.19 | 405.54 | −0.086 |
| 2 | 1 | 474.42 | 474.45 | −0.007 |
| 3 | 1 | 559.37 | 560.73 | −0.244 |
| 4 | 1 | 668.08 | 670.67 | −0.387 |
| 5 | 1 | 782.47 | 787.35 | −0.624 |
| 1 | 2 | 786.74 | 788.04 | −0.166 |
| 2 | 2 | 823.15 | 823.04 | −0.013 |
| 3 | 2 | 877.36 | 879.32 | −0.224 |
| 6 | 1 | 902.13 | 910.04 | −0.877 |
| 4 | 2 | 949.99 | 951.65 | −0.175 |

[a]12-term Rayleigh–Ritz solution. [b]1960-element model.

**Table 4 Comparison of bare membrane and layered membrane systems**

| | | Natural frequency, Hz | | |
|---|---|---|---|---|
| $m$ | $n$ | Bare membrane[b] | Membrane with PVDF patch[c] | Percent difference[a] |
| 1 | 1 | 411.678 | 405.192 | 1.575 |
| 2 | 1 | 475.365 | 474.416 | 0.200 |
| 3 | 1 | 565.797 | 559.365 | 1.137 |
| 4 | 1 | 672.267 | 668.084 | 0.622 |
| 5 | 1 | 788.303 | 782.471 | 0.740 |
| 1 | 2 | 788.303 | 786.735 | 0.199 |
| 2 | 2 | 823.356 | 823.151 | 0.025 |
| 3 | 2 | 878.675 | 877.355 | 0.150 |
| 6 | 1 | 910.254 | 902.126 | 0.893 |
| 4 | 2 | 950.730 | 949.988 | 0.078 |

[a](Bare-patch)/bare.
[b]Exact solution.
[c]12-term Rayleigh–Ritz solution.

ANSYS using the prestressed stiffness matrix. The result of this analysis was a list of natural frequencies for the layered system as well as plots of the mode shapes. These results are compared with those from the Rayleigh–Ritz method in the following section.

#### Numerical Results

The preceding dynamic analysis that led to Eq. (25) was used to formulate the mass and stiffness matrices for a system identical to that modeled in ANSYS. However, the mass densities from Tables 1 and 2 were used on a per-unit-area basis. The numerical results from a *Mathematica* code written to formulate and solve the matrix eigenvalue problem using a 12-term ($M = 6$, $N = 2$) expansion of the eigenfunctions given in Eq. (21) are compared with the converged 1960-element ANSYS model in Table 3.

The close agreement between the Rayleigh–Ritz solution and the ANSYS results using its own membrane elements substantiates the conclusion that traditional membrane theory is unable to capture the stiffness effects of the PVDF patch.

Table 4 shows that the additional mass of the PVDF patch lowered the natural frequencies of the layered system compared to the bare membrane, and this is done without making any discernible change in the mode shapes. Adding a patch increases both mass and stiffness of the section, and these two changes tend to push the natural frequencies in opposite directions. However, the inability of membrane theory to account for the added stiffness leaves only the mass effects on the system.

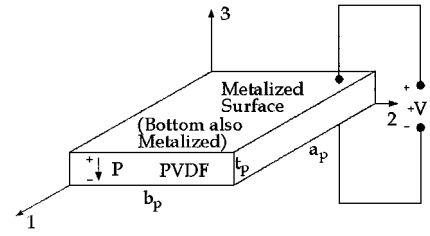


**Fig. 6 Piezoelectric PVDF patch.**

## Active PVDF Patch

The inability of membrane theory to account for the added stiffness of a PVDF patch has been established. This section addresses the ability of membrane theory to model a PVDF as either a sensor or an actuator for an intelligent structure. Figure 6 shows the PVDF patch configured to utilize its piezoelectric nature, where the 1–2 plane is aligned with the $x$–$y$ plane as depicted in Fig. 2.

The active behavior of this patch is governed by the piezoelectric constitutive relationship, given in tensor form as

$$D_i = d_{ijk} T_{jk} + \varepsilon^T_{ij} E_j, \qquad i, j, k = 1, 2, 3 \tag{26}$$

$$S_{ij} = s^E_{ijkl} T_{kl} + d_{kij} E_k, \qquad i, j, k, l = 1, 2, 3 \tag{27}$$

Although this tensor relationship can be somewhat cumbersome, many simplifications can be made to reduce the complexity of Eqs. (26) and (27). First, the base layer and PVDF patch are known to be in a state of plane stress with no in-plane shearing. Therefore, the stress tensor has only two nonzero components. Also, only the electric field applied through the thickness (3-direction) can be nonzero because of the extremely thin nature of the patch. Next, PVDF is a semicrystalline polymer, which means that tiny crystalline regions are connected with amorphous material. These crystalline portions are responsible for the piezoelectric behavior of the polymer and possess a crystal symmetry that reduces the $d$ tensor to only five nonzero components. Furthermore, the PVDF for this paper is considered biaxial, meaning that it was stretched by the same amount in both in-plane orthogonal directions during processing, thus rendering the constants $d_{31}$ and $d_{32}$ equal. After applying these simplifications, the piezoelectric constitutive relationship for this particular application simplifies to

$$D_3 = d_{31}(\sigma_1 + \sigma_2) + \varepsilon_{33} E_3 \tag{28}$$

$$S_1 = (1/Y_P)(\sigma_1 - \nu_P \sigma_2) + d_{31} E_3$$

$$S_2 = (1/Y_P)(\sigma_2 - \nu_P \sigma_1) + d_{31} E_3$$

$$S_3 = -(\nu_P / Y_P)(\sigma_1 + \sigma_2) + d_{33} E_3 \tag{29}$$

where the stresses are found using the step approximation as depicted in Fig. 4.

#### Sensor Applications

Equation (28), which relates the electric displacement (developed charge per unit area) to the applied stress, is referred to as the sensor form of the piezoelectric relationship, where the applied electric field is typically zero. However, voltage is the easiest output to measure from a sensor; the voltage is found by dividing the developed charge by the capacitance of the PVDF. The developed charge is found by integrating the electric displacement over the area of the patch, but under the restrictions of traditional membrane theory the stress values are only caused by the internal pressure of the torus and do not depend on the out-of-plane displacement; thus the predicted voltage output is a constant:

$$V = \frac{d_{31}(\sigma_1 + \sigma_2) a_P b_P}{C_P} \tag{30}$$

However, even this equation is misleading because piezoelectric materials lose their charge quickly, thus making poor static measurement devices. More importantly, because the voltage does not change as the layered system undergoes transverse deflections one concludes that traditional membrane theory is unable to model the PVDF patch as a sensor for out-of-plane vibrations.

**Actuator Applications**

Equation (29) is known as the actuator form of the piezoelectric relationships as it relates applied stresses and electric fields to induced strains. These strains are typically modeled as forces applied at some distance from the middle (neutral) surface of a structure. However, because membranes have no bending stiffness these forces cannot be considered to cause bending. Rather, these piezoelectric strains are represented as in-plane forces applied to the substrate in a manner similar to the pin-force method for beams.[5] Thus another limitation of traditional membrane theory has been uncovered; active patch attachments cannot be modeled to excite transverse vibrations of membranes.

Still hoping for some useful model of patch-structure interaction, these in-plane forces are now considered to be applied at the neutral axis of the base layer so that the tensions in the base layer can be altered as a function of voltage applied to the patch. Assuming displacement continuity between the two rigidly bonded layers, the stresses in the base layer under the patch are given by

$$\sigma_x^b = \sigma_x^{b^{(i)}} + \frac{Y_b d_{31} V}{t_P(1-\nu_b)} \tag{31}$$

$$\sigma_y^b = \sigma_y^{b^{(i)}} + \frac{Y_b d_{31} V}{t_P(1-\nu_b)} \tag{32}$$

where the electric field has been replaced by the voltage divided by the thickness $V/t_P$. Because the substrate must remain a continuous system, it is clear that the base layer away from the patch must undergo a deflection equal in magnitude but opposite in sign to that of the patch and base layer under the patch. The change in strains of the base layer under the patch caused by a voltage applied to the patch are given as

$$\Delta S_x^b = (1/Y_b)\left\{\left(\sigma_x^b - \nu_b\sigma_y^b\right) - \left[\sigma_x^{b^{(i)}} - \nu_b\sigma_y^{b^{(i)}}\right]\right\} \tag{33}$$

$$\Delta S_y^b = (1/Y_b)\left\{\left(\sigma_y^b - \nu_b\sigma_x^b\right) - \left[\sigma_y^{b^{(i)}} - \nu_b\sigma_x^{b^{(i)}}\right]\right\} \tag{34}$$

The changes in strains of the base layer away from the patch are given by similar expressions:

$$\Delta S_y = (1/Y_b)\left\{(\sigma_y - \nu_b\sigma_x) - \left[\sigma_y^{(i)} - \nu_b\sigma_x^{(i)}\right]\right\} \tag{35}$$

$$\Delta S_y = (1/Y_b)\left\{(\sigma_y - \nu_b\sigma_x) - \left[\sigma_y^{(i)} - \nu_b\sigma_x^{(i)}\right]\right\} \tag{36}$$

The last four equations have been for various strain quantities; however, deformation compatibility must be met, and the relationship between strains and deflections for the base layer under and away from the patch are required:

$$\Delta S_x^b = \Delta x^b / a_p, \qquad \Delta S_y^b = \Delta y^b / b_p$$

$$\Delta S_x = \Delta x/(a - a_P), \qquad \Delta S_y = \Delta y/(b - b_P) \tag{37}$$

where $\Delta x^b$ and $\Delta y^b$ are deformations in the base layer under the patch and $\Delta x$ and $\Delta y$ refer to deformations of the base layer away from the patch. Following the equal but opposite deflection argument from the preceding, the deflections can be related, and the unknown stresses $\sigma_x$ and $\sigma_y$ can be solved for simultaneously. Multiplying these stresses by the thickness of the base layer yields tension quantities, which are functions of voltage applied to the patch and given by

$$P_x(V) = \sigma_x^{(i)} t_b + \frac{t_b d_{31} Y_b V}{t_P\left(\nu_b^2 - 1\right)}\left[\frac{a}{a_P} + \frac{\nu_b b}{b_P} - (\nu_b + 1)\right] \tag{38}$$

**Table 5 Voltage limitations and corresponding base-layer tensions**

| Minimum voltage, −61.56 V | | Maximum voltage, 375 V | |
|---|---|---|---|
| $P_x$ | 0 | $P_x$ | 0.93 kN/m (5.32 1b/in.) |
| $P_y$ | 0.131 kN/m (0.75 1b/in.) | $P_y$ | 1.06 kN/m (6.07 1b/in.) |

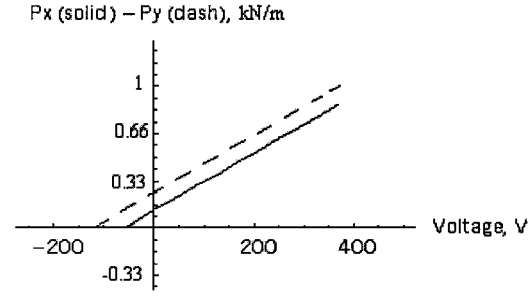


**Fig. 7 Tensions vs voltage applied to PVDF patch.**

$$P_y(V) = \sigma_y^{(i)} t_b + \frac{t_b d_{31} Y_b V}{t_P\left(\nu_b^2 - 1\right)}\left[\frac{\nu_b a}{a_P} + \frac{b}{b_P} - (\nu_b + 1)\right] \tag{39}$$

These expressions possess the general linear relationship $y = b + mx$, where $y$ is voltage-dependent tension, $b$ is the initial tension, $m$ is a combination of material and geometric constants, and $x$ is the applied voltage.

**Numerical Results**

Using the geometric and material properties from Tables 1 and 2 and $d_{31}$ equal to $-2.3 \times 10^{-11}$ m/V ($-9.055 \times 10^{-10}$ in./V), Fig. 7 was constructed showing the linear relationship just predicted.

Despite this linear relationship, there are a few practical limitations to the voltage that can be applied to the patch. First, the patch cannot reduce either tension in the membrane below zero, as membranes cannot support compressive loads without wrinkling. Also, the voltage cannot be applied in excess of the maximum operating voltage lest arcing or depoling could occur. These limitations are summarized in Table 5, along with the attainable values of tensions at such extreme voltages.

These limitations are of key importance to control system designers because they typically want to apply as much voltage as possible to an intelligent structure in an attempt to maximize control authority. Even with these practical limitations, the patch does have a considerable ability to alter the tension in the base layer. Although membrane theory does not allow for the excitation of transverse vibrations, altering the tensions in this manner could be used to quickly damp out vibrations of a layered system.

## Conclusions

With the level of interest in inflatable space-based structures high, a question in the minds or researchers who work with these thin, lightweight high-tech devices might be, "Can these structures be modeled as membranes?" From the results of the current research effort, the answer is "no." Traditional membrane theory was able to account for only the added mass of the patch, not the additional stiffness. This addition of mass resulted in lower natural frequencies; however, the ignored stiffness would tend to raise natural frequencies. Thus the impact on the overall layered system dynamics is inconclusive using traditional membrane theory. However, subsequent work using a more complex thin-plate theory has shown that small PVDF actuators do not alter the natural frequencies in a significant manner.[12] As far as intelligent structures are concerned, the small displacement-constant tension restriction of traditional membrane theory renders the PVDF film useless as a sensor for transverse vibrations. Furthermore, because membranes have no bending stiffness the possibility of exciting transverse vibrations is eliminated, and the amount of control authority is severely restricted. However, in an approach analogous to the pin-force method for bending actuators, membrane theory was able to predict the changes in base layer

tensions as a function of voltage applied to the patch. To improve upon the limitations of membrane theory as it applies to the layering of thin films, it is clear that one must model such systems using thin plate theory, which will allow the tension to change in the film as it undergoes transverse vibrations.

## Acknowledgments

The U.S. Air Force Office of Scientific Research supported this research effort under Grant F49620-99-1-0231. The NASA Virginia Space Grant Consortium Aerospace Graduate Research Fellowship provides additional funding for R. Brett Williams while he completes his graduate education. The financial and technological support of these organizations is gratefully acknowledged.

## References

[1]Main, J. A., Carlin, R. A., Garcia, E., Peterson, S. W., and Strauss, A. M., "Dynamic Analysis of Space-Based Inflated Beam Structures," *Journal of the Acoustical Society of America*, Vol. 97, No. 2, 1995, pp. 1035–1045.

[2]Griffith, D. T., and Main, J. A., "Modal Testing of an Inflated Thin Film Polyimide Torus Structure," *Proceedings, XVIII International Modal Analysis Conference*, Vol. 2, Society of Experimental Mechanics, San Antonio, TX, 2000, pp. 1035–1041.

[3]Coleman, A. D., "Solar Orbital Transfer Vehicle (SOTV), Pathfinder 3 Inflatable Concentrator Modal Survey Under Ambient Conditions,"NASA 98-145, Dec. 1998.

[4]Lummer, D., "Theoretical and Experimental Investigations of Piezoelectric Bending Actuators," M.S. Thesis, Dept. of Mechanical Engineering, Virginia Polytechnic Inst. and State Univ., Blacksburg, VA, Dec. 1998.

[5]Chaudhry, Z., and Rogers, C. A., "The Pin-Force Model Revisited," *Journal of Intelligent Materials Systems and Structures*, Vol. 5, No. 3, 1994, pp. 347–354.

[6]Crawley, E. F., and de Luis, J., "Use of Piezoelectric Actuators as Elements of Intelligent Structures," *AIAA Journal*, Vol. 25, No. 10, 1987, pp. 1373–1385.

[7]Hagood, N. W., Chung, W. H., and von Flotow, A., "Modelling of Piezoelectric Actuator Dynamics for Active Structural Control," *Proceedings of the AIAA/ASME/ASCE/AHS/ASC 31st Structures, Structural Dynamics, and Materials Conference*, AIAA, Washington, DC, 1990, pp. 2242–2256.

[8]Banks, H. T., Smith, R. C., and Wang, Y., "The Modeling of Piezoceramic Patch Interactions with Shells, Plates, and Beams," *Quarterly of Applied Mathematics*, Vol. 53, No. 2, 1995, pp. 353–381.

[9]van Niekerk, J. L., and Tongue, B. H., "Active Control of a Circular Membrane to Reduce Transient Noise Transmission," *Journal of Vibration and Acoustics*, Vol. 117, No. 7, 1995, pp. 252–258.

[10]Agnes, G. S., and Rogers, J. W., "Piezoelectric Excitation of Inflatable Space Structures for Modal Testing," *Smart Structures and Materials 2000: Smart Structures and Integrated Systems*, edited by L. P. Davis, Vol. 3985, *Proceedings of SPIE*, SPIE—International Society for Optical Engineering, Bellingham, WA, 2000, pp. 806–816.

[11]Williams, R. B., "Localized Effects of Piezopolymer Devices on the Dynamics of Inflatable Space-Based Structures," M.S. Thesis, Dept. of Mechanical Engineering, Virginia Polytechnic Inst. and State Univ., Blacksburg, VA, Aug. 2000, URL: http://scholar.lib.vt.edu/theses/available/etd-08152000-16590058/[cited 21 Jan. 2000].

[12]Lewis, J. A., "Finite Element Modeling and Active Control of an Inflated Torus Using Piezoelectric Devices," M.S. Thesis, Dept. of Mechanical Engineering, Virginia Polytechnic Inst. and State Univ., Blacksburg, VA, Dec. 2000, URL: http://scholar.lib.vt.edu/theses/available/etd-12192000-102607/[cited 21 Jan. 2000].

R. B. Malla
*Associate Editor*